ELSEVIER

Contents lists available at ScienceDirect

## **Atmospheric Environment**

journal homepage: www.elsevier.com/locate/atmosenv



# The evolution of physical and chemical properties of $PM_{2.5}$ in the developing stage of pollution events in a coastal megacity, South Korea

Yongmi Park <sup>a</sup>, Myounghwa Byun <sup>a,1</sup>, Jaehun Park <sup>a,2</sup>, Subin Han <sup>a</sup>, Jae-Jin Kim <sup>a</sup>, Youn-Suk Son <sup>b</sup>, Taehyoung Lee <sup>c</sup>, Wonsik Choi <sup>a,d,\*</sup>

- a Major of Environmental Atmospheric Sciences, Division of Earth and Environmental System Sciences, Pukyong National University, Busan, 48513, Republic of Korea
- b Major of Environmental Engineering, Division of Earth and Environmental System Sciences, Pukyong National University, Busan, 48513, Republic of Korea
- Department of Environmental Science, Hankuk University of Foreign Studies, Yongin, 17035, Republic of Korea
- d Research & Management Center for Particulate Matter in the Southeast Region of Korea, Ulsan National Institute of Science and Technology, Ulsan, 44919, Republic of Korea

#### HIGHLIGHTS

- As PM<sub>2.5</sub> increases, a fraction of nitrate linearly increased in a coastal megacity.
- Size of the dominant mode in aerosol surface area grew during pollution periods.
- Peaks in ALWC and RH preceded enhanced nighttime SIA level during pollution periods.
- PM pollution in winter was driven by nocturnal heterogeneous formation of nitrate.

## ARTICLE INFO

Keywords:
Coastal city
PM<sub>2.5</sub>
Aerosol liquid water content
Heterogeneous reaction
Nitrate
Surface area size distribution

## ABSTRACT

Concentrations of  $PM_{2.5}$  (particulate matter smaller than 2.5  $\mu m$  in diameter) vary depending on regional emissions and meteorological conditions. This study investigates the physical and chemical characteristics of  $PM_{2.5}$  and its formation mechanisms in Busan, a coastal megacity in Korea with significant port-related emissions. An increase in  $PM_{2.5}$  concentrations was associated with a rising proportion of nitrate ( $NO_3^-$ ), highlighting the role of nitrate formation in elevated wintertime  $PM_{2.5}$  levels. Throughout the measurement period, an ammonium-rich environment peristed, with the molar ratio of excess- $NH_4^+$  to  $NO_3^-$  approaching 1:1, indicating that the formed nitrates were effectively neutralized by ammonium ions. In diurnal variations during high  $PM_{2.5}^-$  periods, the peak concentrations in  $PM_{2.5}^-$  occurred at night, closely following the daily maxima in relative humidity and aerosol liquid water content (ALWC). Moreover, case studies revealed that increases in relative and specific humidity preceded the augmentation of ALWC, coinciding with the growth of the major aerosol mode larger than 200 nm. This increase in ALWC likely facilitated the efficient conversion of nitrate into a condensed phase, promoting heterogeneous nitrate formation. Consequently, this nighttime heterogeneous formation of nitrate, driven by the increase in ALWC, plays a significant role in the formation of fine particulate matter in a coastal megacity of Korea during winter.

This article is part of a special issue entitled: Study for FRIEND project published in Atmospheric Environment.

<sup>\*</sup> Corresponding author. Major of Environmental Atmospheric Sciences, Division of Earth and Environmental System Sciences, Pukyong National University, Busan, 48513, Republic of Korea.

E-mail addresses: ygm23@pukyong.ac.kr (Y. Park), bmh3901@korea.kr (M. Byun), jhpark0812@kist.re.kr (J. Park), sbhan@pukyong.ac.kr (S. Han), jjkim@pknu.ac.kr (J.-J. Kim), sonys@pknu.ac.kr (Y.-S. Son), thlee@hufs.ac.kr (T. Lee), wschoi@pknu.ac.kr (W. Choi).

<sup>&</sup>lt;sup>1</sup> Current affiliation: Climate and Air Quality Research Department, National Institute of Environmental Research (NIER), Incheon, Republic of Korea.

<sup>&</sup>lt;sup>2</sup> Current affiliation: Climate & Air Policy Team, Clean Air Center, Korea Institute of Science and Technology, Seoul, 02792, Republic of Korea.

## 1. Introduction

The annual average concentration of  $PM_{2.5}$  (particulate matter smaller than 2.5  $\mu m$  in diameter) in South Korea was recorded at 18  $\mu g$   $m^{-3}$  in 2021, marking a decrease from 26  $\mu g$   $m^{-3}$  reported in 2015 when  $PM_{2.5}$  monitoring was initiated (National institute of environmental research (NIER), 2021). Despite these improvements, only 24.3 % of monitoring stations in 2021 met the annual environmental standard of 15  $\mu g$   $m^{-3}$  or lower, highlighting that the majority of regions still surpassed the standard (National institute of environmental research (NIER), 2021). While the South Korean government has implemented seasonal PM management strategies since 2019 to reduce  $PM_{2.5}$  concentrations (Ministry of Environment (ME), 2019), ongoing reductions in emissions are essential to meet the government's target of an annual average  $PM_{2.5}$  concentration of 13  $\mu g$   $m^{-3}$  by 2027.

PM<sub>2.5</sub> consists of a complex mixture of organic and inorganic materials, elemental carbon, and others. On average, sulfates, nitrates, and ammonium account for 30-50 % of the PM<sub>2.5</sub> mass concentration in South Korea's metropolitan areas (Bae et al., 2020; Han and Kim, 2015). Kim et al. (2022) found that secondary aerosols contributed up to 77 % of the total PM<sub>2.5</sub> during high pollution episodes in Seoul. Similarly, secondary inorganic aerosols (SIA) significantly influence PM<sub>2.5</sub> levels in China, comprising 25-60 % of the PM<sub>2.5</sub> mass (Wang et al., 2018; Ye et al., 2017). Following the enforcement of strict regulations, China has achieved significant reductions in SO2 and NOx emissions, the primary precursor gases for PM<sub>2.5</sub> (Vu et al., 2019; Wang et al., 2022). As a result, SO<sub>2</sub> and NOx emissions decreased by 68 % and 17 %, respectively, between 2013 and 2017 (Vu et al., 2019; Zheng et al., 2018). The more substantial reduction in SO2 emissions compared to NOx has enhanced the role of nitrates over sulfates during periods of high PM2.5 concentrations (Lin et al., 2020; Xu et al., 2019). Previous studies have reported that these emission reductions in China have resulted in decreased SO<sub>2</sub> levels and increased nitrates in South Korea, situated downwind of the Asian continent (Jo et al., 2020; Uno et al., 2020). Recent findings also suggest a shift in the inorganic composition in Seoul, with a decrease in the proportion of sulfates and an increase in nitrates in PM2.5 (Hwang et al., 2023; Kim et al., 2022; Lee et al., 2023).

Bae et al. (2022) suggested that the annual contribution of transboundary transport to  $PM_{2.5}$  levels in South Korea decreased from 52 % in 2015 to 43 % in 2020. These results suggest that as foreign emissions diminish,  $PM_{2.5}$  concentrations in each region of Korea may become more influenced by local emissions and meteorological conditions. Therefore, to understand the spatiotemporal variability of  $PM_{2.5}$  in South Korea and to identify the drivers of  $PM_{2.5}$  formation and growth in each region, understanding the chemical and physical properties of fine particles affected by local emissions characteristics is required.

Zhou et al. (2022) reported that from 2011 to 2019, while NOx and PM<sub>2.5</sub> concentrations decreased in eastern China, the nitrate concentrations in PM<sub>2.5</sub> remained nearly unchanged. They attributed the increased proportion of nitrates to enhanced N<sub>2</sub>O<sub>5</sub> formation during the night, driven by rising ozone levels and decreasing NO concentrations. Zang et al. (2022) found that in the Yangtze River Delta (YRD), nitrates were produced at rates of 3.81 μg m<sup>-3</sup>·h<sup>-1</sup> during the night through the heterogeneous hydrolysis of N<sub>2</sub>O<sub>5</sub> and at 2.61 μg m<sup>-3</sup>·h<sup>-1</sup> during the daytime through the gas-phase reaction of  $OH + NO_2$ . These processes accounted for 66 % and 32 % of nitrate formation in the YRD during winter, respectively. Kim et al. (2022) identified sulfates as the most significant component of SIA in PM1 in South Korea's metropolitan areas, followed by nitrates, which constituted approximately 20 %. However, Kang et al. (2022) noted that nitrate concentrations were predominant when  $PM_{2.5}$  exceeded 35 µg m<sup>-3</sup>, the national air quality standard.

Nonetheless, most research on  $PM_{2.5}$  formation and growth in South Korea has predominantly focused on the metropolitan areas, while studies in coastal cities like Busan have been scarce. Kim et al. (2020) observed that from 2015 to 2018, the ratio of nitrate to sulfate

concentrations in  $PM_{2.5}$  was approximately 0.43 in Seoul and 0.25 in Busan, indicating that nitrogen oxides were a major factor in  $PM_{2.5}$  formation in Seoul, whereas sulfur oxides played a more significant role in Busan. To reduce  $SO_2$  emissions, large vessels in Busan's ports have been mandated to operate at reduced speeds (below 12 knots) since September 2020, under the Enforcement Decree of the Special Act on the Improvement of Air Quality in Port Areas (Ministry of Oceans and Fisheries (MOF), 2019). Furthermore, the sulfur content in marine fuel has been regulated to be below 0.1 %, stricter than the international limit of 0.5 % (Ministry of Oceans and Fisheries (MOF), 2019).

These policies are expected to decrease  $SO_2$  emissions from ship and port operations, potentially altering the proportion of sulfates in  $PM_{2.5}$  in coastal cities like Busan. This change may also influence the increased contribution of nitrates in these areas. Consequently, this study aimed to reevaluate the physicochemical properties of  $PM_{2.5}$  in South Korea's coastal megacities, such as Busan, where research has been relatively limited and where large ports, small industrial areas, and dense road networks coexist. The study also sought to understand the physicochemical mechanisms leading to high  $PM_{2.5}$  concentrations.

#### 2. Methods

#### 2.1. Sampling site and instrumentation

Field measurements were conducted at the Yongdang campus of Pukyong National University, located in Nam-gu, Busan (35.114° N, 129.089° E; Fig. 1). The Busan Institute of Health & Environment Research operates three monitoring sites in Busan to measure  $PM_{2.5}$  chemical components (Fig. 1b). However, all these sites are situated at ground level, primarily to monitor primary emissions from different sources (port, industry, and mobile sources), and are thus directly influenced by proximate emission sources.

In contrast, the Yongdang campus is situated on a foothill approximately 1 km from the coast, free from any obstructions to airflow (elevation 65 m above sea level). The site is also relatively unaffected by specific emission sources, making it suitable for analyzing the local pollutant characteristics influenced by seasonal variations. Nevertheless, the characteristic urban environment of a port city places small industrial facilities about 1 km west of the measurement site, a commercial area 1 km to the north, and a port 0.6 km to the south (Fig. 1c). This complex urban mixture, combining emissions from roads, commercial areas, ships/ports, and small industries, typifies the emission environments in Busan.

Winter was selected as the measurement period because frequent air stagnation and higher  $PM_{2.5}$  concentrations occur during this season compared to others, making it particularly suitable for studying the evolution of the physical and chemical properties of  $PM_{2.5}$ . Measurements were conducted from January 13 to February 7, 2021.

Inorganic ion components of PM<sub>2.5</sub> (Na<sup>+</sup>, NH<sub>4</sub><sup>+</sup>, K<sup>+</sup>, Ca<sup>2+</sup>, Mg<sup>2+</sup>, F<sup>-</sup>, Cl<sup>-</sup>, NO<sub>3</sub>, SO<sub>4</sub><sup>2-</sup>) were measured using a particle into liquid sampler-ion chromatography (PILS-IC) system. Air samples were collected at a constant flow rate of 16.7 L min<sup>-1</sup> using a PM<sub>2.5</sub> cyclone (URG-2000-30EH). To minimize further gas-particle reactions, the samples passed through an annular denuder coated with phosphorus acid and sodium carbonate (URG Corp.) to remove gaseous HNO3 and NH3. The particles injected into the PILS underwent liquefaction upon exposure to 150 °C high-temperature steam generated by the Steamer. These liquid particles were then collected on the impactor plate, along with the carrier solution. We analyzed the collected sample at approximately 30-min intervals using ion chromatography (IC, Eco IC 925, Metrohm Corp.). The IC separated each ion component through a fixed-phase column (anions: Metrosep A Supp 5-150/4.0; cations: Metrosep C4-150/4.0) and an eluent (anions: Na<sub>2</sub>CO<sub>3</sub> 64 mM & NaHCO<sub>3</sub> 20 mM; cations: HNO<sub>3</sub> 34 mM & dipicolinic acid 14 mM). The flow rates for anions and cations in the IC were set at 0.9 and 0.7 mL min<sup>-1</sup>, respectively (Metrohm Corp.). Before the field campaign, we performed a multipoint

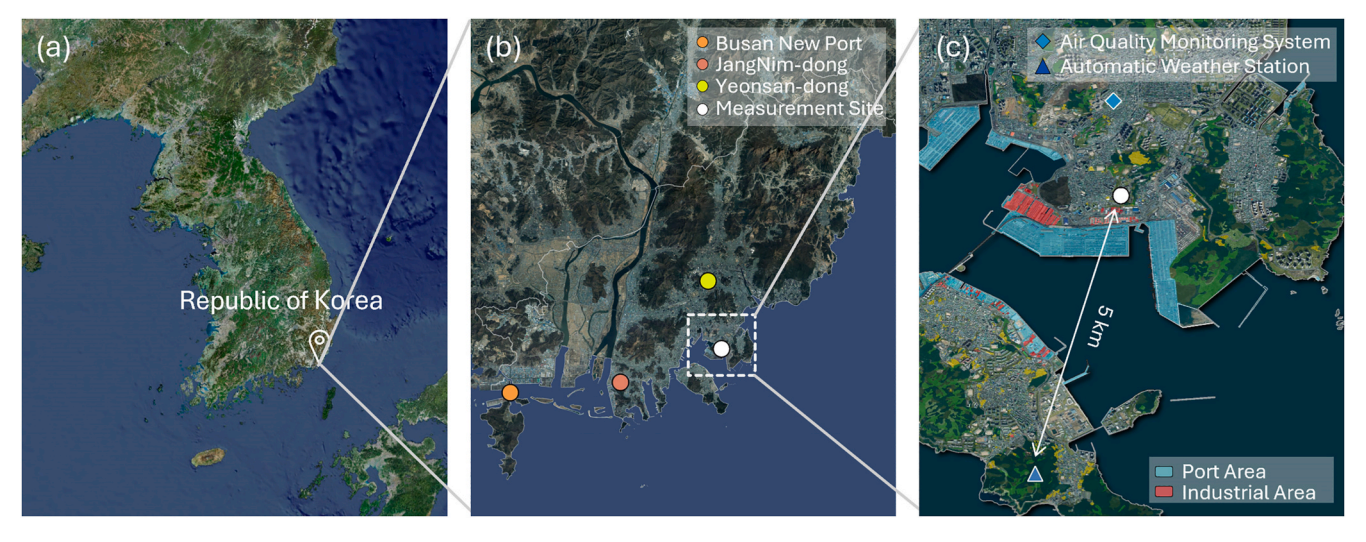


**Fig. 1.** Map of the measurement site. (a) Republic of Korea, (b) PM<sub>2.5</sub> component monitoring sites in Busan (Orange: Busan New port, Red: JangNim, Lime green: Yeonsan) and the measurement site in this study (white circle), (c) The surrounding environments of the measurement site (Sky-blue: port area, Red: industrial areas). Sky-blue diamond and blue triangle denote air quality monitoring station (AQMS) and automatic weather station (AWS) site, respectively.

calibration using a 100 ppm standard solution containing all target ions (Sigma-Aldrich Corp.), which was diluted into four different concentrations. This calibration converted the areas of the ion component chromatograms into concentrations (Supplementary Information (SI), Fig. S2). Additionally, the dilution factor calculated using a LiBr solution was applied to convert into mass concentrations (SI, Fig. S3). More details for the PILS-IC method are available elsewhere (Kang et al., 2020; Lee et al., 2008; Park et al., 2014). The method detection limit (MDL) estimated with 19 blank samples were 0.52, 0.01, 0.02, 0.02, and 0.01  $\mu g \ m^{-3}$  for Na $^+$ , NH $^+_4$ , K $^+$ , Ca $^{2+}$ , and Mg $^{2+}$ , respectively at the t-value for a 99 % confidence level. For anions (F $^-$ , Cl $^-$ , NO $^-_3$ , SO $^{2-}_4$ ), the MDL converged to zero due to the suppressor installed to reduce instrumental noise.

To analyze the growth of  $PM_{2.5}$  and the gas-to-particle conversion, we simultaneously measured precursor gas concentrations (NH<sub>3</sub>, NO, NO<sub>2</sub>, and SO<sub>2</sub>) and particle size distributions (Table 1). NO<sub>X</sub> and NH<sub>3</sub> concentrations were measured using a NO<sub>X</sub>/NH<sub>3</sub> Gas Analyzer (17C NO-NO<sub>2</sub>-NO<sub>X</sub> Analyzer with 17C NH<sub>3</sub> converter, Thermo Scientific Inc.), and zero and span calibrations for NO<sub>X</sub> and NH<sub>3</sub> were performed prior to the field measurements. Particle size distributions were measured using a

Table 1
Measurements used in this study.

Compound	Instrument	Frequency
Particle-phase species		
PM <sub>2.5</sub> components (NH <sub>4</sub> <sup>+</sup> , SO <sub>4</sub> <sup>2-</sup> , NO <sub>3</sub> <sup>-</sup> , Cl <sup>-</sup> ,Na <sup>+</sup> , Ca <sup>2+</sup> , K <sup>+</sup> , Mg <sup>2+</sup> , F <sup>-</sup> )	particle into liquid sampler-ion chromatography (PILS-IC)	30 min
Number concentration (12.6 nm–10 mm)	scanning mobility particle sizer (SMPS) $+$ optical particle sizer (OPS)	2 min
PM <sub>2.5</sub> Mass concertation	From national air quality monitoring station (AQMS)	60 min
Gas-phase species		
NO, NO <sub>2</sub> , NH <sub>3</sub>	17C NO-NO <sub>2</sub> -NOx Analyzer with 17C NH <sub>3</sub> converter	10 s
$SO_2$	43C SO <sub>2</sub> Analyzer	10 s
$O_3$	From AQMS	60 min
Meteorology		
Temperature(T),Relative Humidity(RH)	From automatic weather station (AWS)	1 min

scanning mobility particle sizer (SMPS 3938, TSI) and an optical particle sizer (OPS 3330, TSI) that detect particle numbers for diameters ranging from 12.8 nm to 10  $\mu$ m. PM<sub>2.5</sub> mass and O<sub>3</sub> concentrations were obtained from a government-operated air quality monitoring station (AQMS) located 1.8 km north of the measurement site. Temperature and humidity data were acquired from an automatic weather station (AWS) in Yeongdo-gu, located 5 km southwest of the site.

In Section 3.5 of the results, missing values that occurred in the inorganic ion components during the case study period were replaced with the average values from the Yeonsan-dong and Busan New Port monitoring stations, operated by the Busan Institute of Health & Environment Research, because the measurement site is situated between two stations (SI, Fig. S4) and a comparison of the measured values among sites agreed reasonably for nitrate, sulfate, and ammonium (SI, Fig. S5).

## 2.2. ISORROPIA-II model

We used the ISORROPIA-II model to calculate pH and aerosol liquid water content (ALWC). ISORROPIA-II is an atmospheric thermodynamic model that predicts the formation of substances by assuming thermodynamic equilibrium in the atmosphere (Fountoukis and Nenes, 2007). Bian et al. (2014) reported that the model tends to underestimate ALWC compared to observations under low relative humidity conditions, while the model results agreed well with observations when relative humidity exceeds 60 %. The model inputs included particulate inorganic ions (NH $_4^+$ , NO $_3^-$ , SO $_4^{2-}$ , Cl $^-$ , K $^+$ , Ca $_2^{2+}$ , Mg $_2^{2+}$ ), relative humidity, and temperature.

The model provides two options: forward and reverse modes. The forward mode calculates equilibrium partitioning using precursor gases and inorganic ions concentrations, relative humidity, and temperature, while the reverse mode generates results based primarily on condensed phase ion composition. We selected the forward mode for this study, as it is considered more robust against measurement errors compared to the reverse mode (Guo et al., 2015; Hennigan et al., 2015). The model is further classified as either stable or metastable mode depending on the saturation state. The stable mode assumes that salts precipitate when the liquid aerosol becomes saturated, while the metastable mode assumes that supersaturated aerosols can exist (Fountoukis and Nenes, 2007). Model evaluations suggested that the metastable mode is more reliable than the stable mode (Guo et al., 2017; Wang et al., 2018). In this study, gas-phase HNO<sub>3</sub> was not measured. However, Hennigan et al. (2015) noted that while the reverse mode is typically employed when data on

precursor gases are unavailable, estimates of aerosol pH and ALWC derived from this mode are highly sensitive to even minor measurement uncertainties. Previous studies have also shown that, in the absence of gas-phase data, using only particle-phase concentrations and meteorological factors as inputs in the forward mode provided a more reliable alternative for aerosol pH predictions (Fang et al., 2025; Guo et al., 2015; Hennigan et al., 2015; Zhang et al., 2023). Fang et al. (2025) reported that model calculations underestimated pH by approximately 0.5 units when NH3 concentrations were excluded, yet maintained a strong correlation (R2 > 0.92) with cases including NH3. A similar trend was observed in Bougiatioti et al. (2016). Moreover, since ISORROPIA-II calculates water uptake based on the Zdanovskii-Stokes-Robinson (ZSR) mixing rule (Fountoukis and Nenes, 2007), uncertainties in NH<sub>3</sub> and HNO3 concentrations are unlikely to substantially affect the water content of inorganic species (Wi) (Seo et al., 2020). In this study, ISORROPIA-II model calculations for NH<sub>4</sub>, NO<sub>3</sub>, and SO<sub>4</sub><sup>2-</sup> concentrations exhibited strong agreement with measured values (R<sup>2</sup> > 0.98), suggesting that potential errors in W<sub>i</sub> for individual inorganic species would be minimal. This high correlation further indicates that model uncertainties are likely to have a negligible impact on the key findings of this study. Therefore, the ISORROPIA-II model was applied in the metastable and forward modes to calculate aerosol pH and ALWC in PM<sub>2.5</sub> for this study.

#### 2.3. Separation of aerosol modes from surface area size distributions

In urban areas, aerosol size distributions with diameters below 300 nm vary significantly in both time and space due to various environmental factors, such as direct emissions from local combustion sources, new particle formation, and meteorological conditions (Choi and Paulson, 2016). Therefore, separating and analyzing different modes within the aerosol size distribution is useful to understand the physical evolution of PM<sub>2.5</sub> during particle formation events. Typically, the size distribution of fine particles consists of nucleation mode, Aitken mode, and accumulation mode, each following a log-normal distribution (Seinfeld and Pandis, 2016). Previous studies have employed multi-log-normal distribution functions to quantitatively extract aerosol modes from observed size distributions through the fitting method (Hussein et al., 2005; Seinfeld and Pandis, 2016). In this study, we applied the same approach to extract modes from the aerosol size distribution using Eq. (1) (Hussein et al., 2005):

$$f = \sum_{i=1}^{n} \frac{N_i}{\sqrt{2\pi} log \left(\sigma_{pg,i}\right)} exp \left\{ -\frac{\left[log(D_p) - log \overline{D}_{pg,i}\right]^2}{2 log^2(\sigma_{pg,i})} \right\}, \tag{1}$$

where i represents each mode,  $D_p$  is the particle diameter (nm), N is the number concentration (cm $^{-3}$ ),  $\overline{D}_{pg}$  denotes the geometric mean diameter of the particles (nm), and  $\sigma_{pg}^2$  represents the geometric variance, treated as a free variable in this analysis. The mode extraction process began by assuming that the measured size distribution consisted of three lognormal distribution modes, and we set initial variables using nonlinear least-squares curve fitting with three log-normal distribution functions (n = 3 in Eq. (1)). Subsequently, we conducted iterative calculations using the initial values to derive the convergence values. Finally, we assessed the overlap hypothesis between modes to evaluate the possibility of reducing the number of modes. If two adjacent modes could be integrated into a single mode, one mode was removed since the primary purpose of the fitting process was to determine the parameters that best represented the measured size distributions with the fewest necessary modes, thereby allowing practical tracking of changes in the properties of each mode.

We applied this method separately to the size distributions from both the SMPS and OPS. Subsequently, we combined the modes obtained from the SMPS and OPS size distributions, capturing the entire range of size distributions (12.6 nm–10  $\mu$ m). Then, we adjusted overlapping size

distributions between the SMPS and OPS by aligning the mode diameters from the OPS with those of the SMPS (Khlystov et al., 2004). Consequently, reconstructed size distributions from extracted modes agreed well with measured data, exhibiting high linearity with  $R^2 = 0.997$  (SI, Fig. 6). For further validation, we applied this method to the dataset used by Hussein et al. (2005) and compared the results with those from Hussein et al. (2005). The extracting method used in this study showed improved performance compared to the previous study (SI, S1). Thus, the individual modes extracted from the observed size distributions were used to examine the evolution of the physical properties of  $PM_{2.5}$  in the initial stage of pollution events in this study.

#### 3. Results

#### 3.1. Overview

During the measurement period, PM<sub>2.5</sub> mass concentrations varied between 2  $\mu g~m^{-3}$  and 80  $\mu g~m^{-3}$  , with an average of 19  $\pm$  13  $\mu g~m^{-3}$  . The majority of PM<sub>2.5</sub> concentrations in Busan fell within the Ministry of Environment's standards for "good" (below 15 μg m<sup>-3</sup>) and "moderate" (below 35  $\mu$ g m<sup>-3</sup>) levels, representing 87 % of the observation period. In South Korea, high PM2.5 concentrations are defined as those exceeding 35 µg m<sup>-3</sup>. For this study, we identified high-concentration periods as those during which PM2.5 concentrations exceeded 35 µg m<sup>-3</sup> for longer than two consecutive hours. Throughout the measurement period, four high-concentration events were recorded (Fig. 2, shades of gray). In most high-concentration cases, the concentrations of precursor gases such as NO<sub>X</sub>, NH<sub>3</sub>, and SO<sub>2</sub> also increased, implying that the accumulation of locally emitted precursor gases was one of the causes of the PM<sub>2.5</sub> elevation. During periods of high PM<sub>2.5</sub> concentrations, ALWC consistently showed an increasing trend, underscoring a relationship between PM<sub>2.5</sub> growth and ALWC levels (Fig. 2). Ammonium ion concentrations ranged from 0.1  $\mu g \ m^{-3}$  to 15  $\mu g \ m^{-3}$ , with an average of 3  $\pm$  2  $\mu g\ m^{-3}.$  Nitrate concentrations, a significant component of PM<sub>2.5</sub>, ranged from 0.2  $\mu g$  m<sup>-3</sup> to 42.7  $\mu g$  m<sup>-3</sup>, with an average of 4  $\pm$  6  $\mu g~m^{-3}.$  Sulfate ion concentrations spanned from 0.5  $\mu g~m^{-3}$  to 11 µg m<sup>-3</sup>, with an average of  $3 \pm 2$  µg m<sup>-3</sup>. Typically, the ratios of nitrate to sulfate in PM<sub>2.5</sub> vary seasonally. As temperatures decrease, the equilibrium constant for the reaction between precursor gases (HNO<sub>3</sub>(g) and NH<sub>3</sub>(g)) to form their particulate counterpart (R1) decreases, favoring the formation of nitrates. Low winter temperatures facilitated nitrate formation, partly contributing to its predominance over sulfate concentrations when PM<sub>2.5</sub> concentrations exceeded 20–30  $\mu g m^{-3}$ during the measurement period (Figs. 2 and 3).

$$HNO_{3(g)} + NH_{3(g)} \leftrightarrow NH_4NO_{3(s,aq)} (R \ 1)$$

When comparing the composition ratios of inorganic ions across different PM<sub>2.5</sub> concentration ranges (Fig. 3), the proportion of sulfate decreased with rising PM2.5 levels (Fig. 3b), while the proportion of nitrate correspondingly increased (Fig. 3a). As PM<sub>2.5</sub> concentrations rose, the fractions of crustal or sea salt components also decreased, indicating that increased PM2.5 concentrations were associated with augmented secondary formation of nitrate. In South Korea, the Enforcement Decree of the Special Act on the Improvement of Air Quality in Port Areas in 2020 (Ministry of Oceans and Fisheries (MOF), 2019) led to a reduction in the annual average SO<sub>2</sub> concentration from 5 ppb in 2019 to 3 ppb in 2021 (National institute of environmental research (NIER), 2021; National institute of environmental research (NIER), 2019). In regions such as Europe and China where SO<sub>2</sub> emissions have decreased, nitrate has become a dominant component of SIAs and its contribution is becoming increasingly significant (Erisman and Schaap, 2004; Lin et al., 2020). Similarly, the findings in Fig. 3 suggest that in Korean port cities, like Busan, the contribution of NO<sub>3</sub> to PM<sub>2.5</sub> levels increased more than that of SO<sub>4</sub><sup>2-</sup> as PM<sub>2.5</sub> concentrations rise, implying that  $NO_{3}^{-}$  plays a key role in increasing  $PM_{2.5}$  levels. The

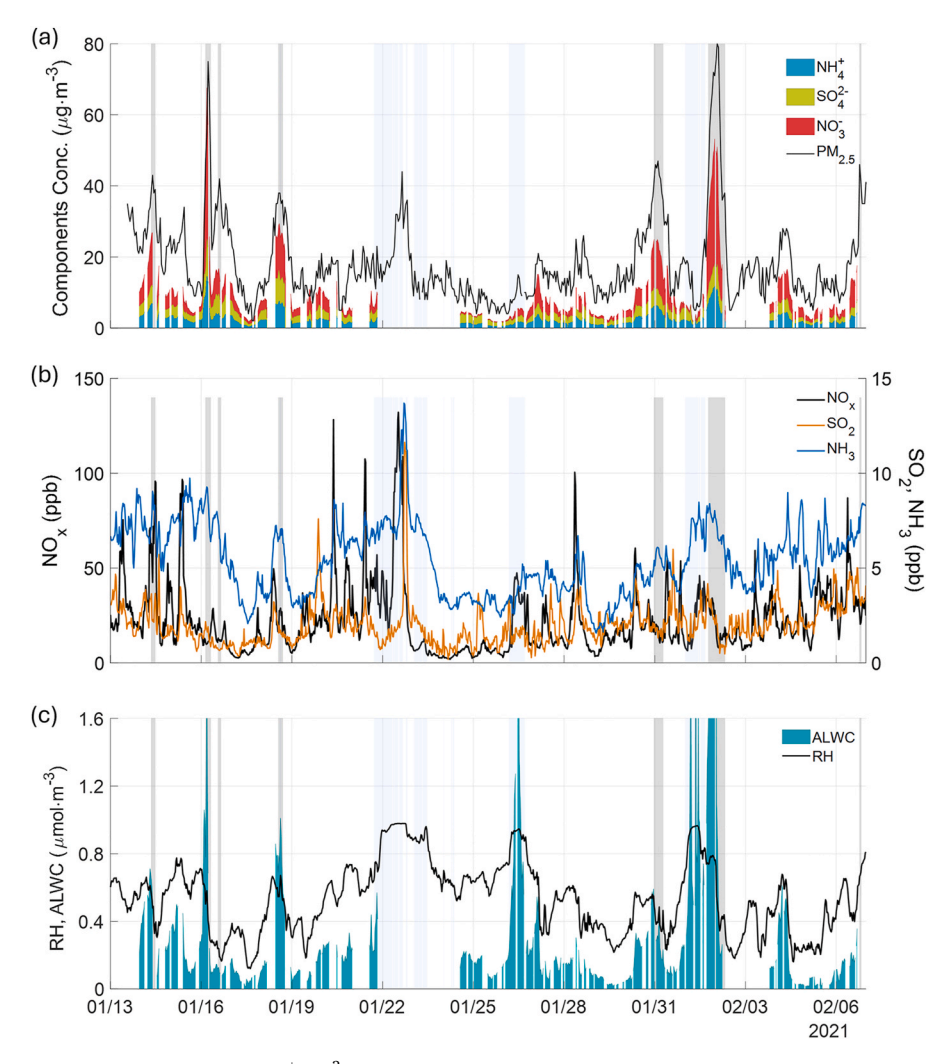


Fig. 2. Time series of concentrations in (a)  $PM_{2.5}$  mass,  $NH_4^+$ ,  $SO_4^{2-}$ ,  $NO_3^-$ . (b) precursor gases ( $NOx(=NO+NO_2)$ ,  $SO_2$ ,  $NH_3$ ). (c) ALWC and RH during the sampling periods. The gray shadows represent the high  $PM_{2.5}$  periods.

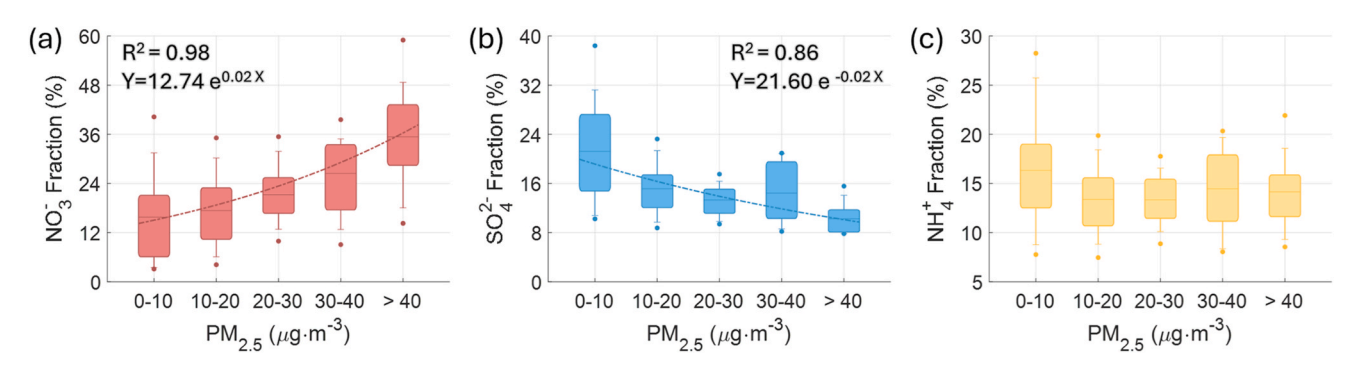


Fig. 3. Fractions of ion components relative to total  $PM_{2.5}$  concentrations, as a function of varying  $PM_{2.5}$  levels: (a) nitrate  $(NO_3^-)$ , (b) sulfate  $(SO_4^{2-})$ , (c) ammonium  $(NH_4^+)$ . The dashed line represents an exponential fit to the data.

proportion of ammonium ions remained relatively steady with respect to  $PM_{2.5}$  concentrations. Thermodynamically, ammonia prefers to neutralize sulfate before nitrate (Ge et al., 2017; Squizzato et al., 2013). Hence, the proportion of ammonium ions remained relatively constant across  $PM_{2.5}$  concentration ranges, neutralizing sulfate at lower  $PM_{2.5}$  concentrations and nitrate at higher concentrations.

## 3.2. Chemical characteristics of SIA

Ammonium ions are one of the major components in atmospheric  $PM_{2.5}$ , neutralizing anions such as nitrates, sulfates, and chlorides. Previous studies have suggested that a molar ratio of  $[NH_{+}^{+}]/[SO_{4}^{2}^{-}]$  above 1.5 signifies an ammonium-rich environment, while the ratio below 1.5 indicate ammonium-poor conditions (Huang et al., 2011; Seinfeld and Pandis, 2016). This ratio is used to determine the pathway of  $NH_{4}NO_{3}$  formation under various environmental conditions

(Squizzato et al., 2013). As depicted at the x-intercept in Fig. 4a, when the [NH<sub>4</sub>]/[SO<sub>4</sub><sup>2-</sup>] ratio exceeds 1.5, ammonia predominantly reacts with gaseous nitric acid to form NH<sub>4</sub>NO<sub>3</sub> (Huang et al., 2011). Conversely, when this ratio is below 1.5, nitrate formation is independent of ammonium, through reactions between HNO3 and sea salt particles (NaCl) or crustal particles (e.g., CaCO<sub>3</sub>) (Arsene et al., 2011; Goodman et al., 2000; Huang et al., 2011). Recent findings, however, have suggested that even in ammonium-rich environments, gaseous N<sub>2</sub>O<sub>5</sub> can dissolve into liquid aerosols and undergo hydrolysis to produce liquid-phase nitrate, contributing significantly to nighttime nitrate formation (Lin et al., 2020; Peng et al., 2021). Throughout the observation period, the molar ratio of  $[\mathrm{NH_4^+}]/[\mathrm{SO_4^{2-}}]$  consistently exceeded 1.5, indicating ammonium-rich conditions. Additionally, the distributions of molar ratios of  $[NO_3^-]/[SO_4^{2-}]$  vs.  $[NH_4^+]/[SO_4^{2-}]$  were consistent with the regression line proposed by Pathak et al. (2009), which was obtained from observations in various cities (Fig. 4a).

Guo et al. (2016) found that as particle pH increases, the proportion of particulate nitrate ( $[NO_3^-]_p$ ) relative to the total nitrate ( $[HNO_3]_g$  +  $[NO_3^-]_p$ ) increases, with most nitrates existing in particulate form above a certain pH level. Since it is difficult to directly measure particle acidity, we employed an ion balance of inorganic components as an indirect acidity indicator (Pathak et al., 2004a, 2004b; Zhang et al., 2007). A commonly used indicator is the concentration of hydrogen ions in particles per unit volume of air (H + aer) (Zhang et al., 2007). The slope of H aer concentration relative to SO<sub>4</sub><sup>2-</sup> concentration was 0.1, suggesting that most sulfate was present as (NH<sub>4</sub>)<sub>2</sub>SO<sub>4</sub> (Fig. 4b). In addition, as pH values, calculated using the ISORROPIA-II model, increased, the relationship between H  $^{+}$  aer and  $SO_4^{2-}$  approached Y = 0, indicating that sulfate was fully neutralized (Fig. 4b). The remaining ammonium, after neutralizing sulfate ions, is referred to as excess-NH<sub>4</sub>, which represents the amount of ammonium exceeding a  $[NH_4^+]/[SO_4^{2-}]$  molar ratio of 1.5 (Eq. (2) (Pathak et al., 2009)). Integrating the results of previous studies conducted in regions such as Hong Kong, Beijing, the United States, and Europe, Pathak et al. (2009) determined that the nitrate formation pattern shifts at a threshold molar ratio of  $[NH_4^+]/[SO_4^{2-}] = 1.5$ , and this definition has been used in several subsequent studies to investigate the role of ammonium in nitrate formation [e.g., 11, (Chen et al., 2024), (Griffith et al., 2015)]. Our results also showed that the molar ratio of excess-NH<sub>4</sub> to NO<sub>3</sub> closely approached a 1:1 line (Fig. 4c), indicating that sufficient NH3 was present to neutralize sulfates and nitrates.

$$Excess|NH_4^+| = (|SO_4^{2-}|/|NH_4^+| - 1.5) \times |SO_4^{2-}|$$
 (2)

In summary, during the winter measurement period, lower temperatures reduced the equilibrium constant ( $K_P$ ) for the reaction between gaseous HNO $_3$  and NH $_3$ , favoring the partitioning of nitrate into the particulate phase, which promoted the formation of NH $_4$ NO $_3$  under

ammonium-rich conditions [36] Furthermore, the pH values calculated using the model appeared to be high when concentrations of nitrate and excess-NH<sub>4</sub><sup>+</sup> were elevated, suggesting that a higher pH environment was more favorable for nitrate to exist in the particulate phase rather than the gaseous phase. The main factors contributing to the increase in pH in Busan during winter appear to be low temperatures, high humidity, NH<sub>3</sub>, and aerosol liquid water content (ALWC). Enhanced NH<sub>4</sub>NO<sub>3</sub> concentrations, which have lower acidity compared to sulfate, reduce the concentration of H<sup>+</sup> and lead to a rise in aerosol pH [30]In addition, the formation of NH<sub>4</sub>NO<sub>3</sub> can further enhance ALWC [ (Guo et al., 2018),(Gysel et al., 2007)], which dilutes more H<sup>+</sup> and further raises the aerosol pH [34,54]. Applying the same methodology as Guo et al. [30] and Nenes et al. (2020)]we examined the relationship between aerosol pH and the nitrate partitioning ratio,  $\varepsilon(NO_3^-) = [NO_3^-]_p/([NO_3^-]_p + [NO_3^-]_g)$ , where p and g denote the particle and gas phases, respectively, across different ALWC concentration ranges within the observation ranges of various input variables during the measurement period using

 $\lfloor NO_3^- \rfloor_g$ ), where p and g denote the particle and gas phases, respectively, across different ALWC concentration ranges within the observation ranges of various input variables during the measurement period using the ISORROPIA-II model. The results showed that  $\varepsilon(NO_3^-)$  follows a sigmoidal function (Eq. S1)shifting rapidly from near zero to one within a specific pH range as Guo et al. [30] presented. Under conditions of high ALWC, the transition of nitrate to the particulate phase occurs more substantially as pH increases, with  $\varepsilon(NO_3^-)$  approaching one at lower pH levels (SI, Fig. S7). Consequently, we conclude that an increase in aerosol pH and ALWC under the low temperatures and ammonia-rich conditions in the coastal megacity of South Korea further enhanced the formation of particulate NO $_3^-$  [ (Guo et al., 2016), (Liu et al., 2017)].

According to national emissions statistics, 51 % of total  $NH_3$  emissions in the Busan area originate from 'other non-point pollutant sources', and this proportion increases to 81 % in Nam-gu, a sub-district of Busan where the measurement site is located (CAPSS and https, 2022). This category of area sources includes emissions from vegetations, soils, wildfires, and others. However, the results of the conditional probability function (CPF) analysis, which shows the wind-directional distribution of high concentrations of  $NH_3$  during the measurement period, indicate that relatively elevated  $NH_3$  levels originated from the direction of the port and ocean, implying potential contributions from ship operations and industrial activities to ammonium-rich environments in the study area (SI, Fig. S8). Nonetheless, in such complex environments where diverse non-point sources are mixed, identifying specific  $NH_3$  emission sources is challenging and is beyond the scope of this study.

## 3.3. Diurnal variations

The diurnal variations of observed species during low to moderate PM<sub>2.5</sub> concentration periods (excluding days when PM<sub>2.5</sub> levels

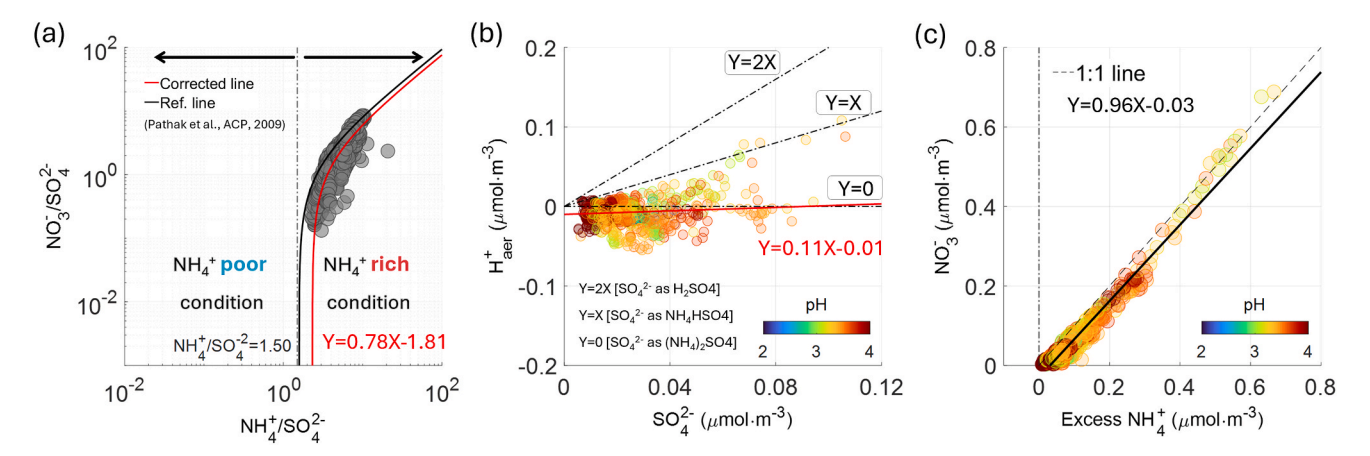


Fig. 4. (a) Determining the Ammonium condition through comparison of molar ratios of  $NO_3^-/SO_4^{2-}$  and  $NH_4^+/SO_4^{2-}$ . (b) The molar ratio of  $H_{aer}^+$ , the calculated concentration of hydrogen ions within the particle, and  $SO_4^{2-}$ . (c) The molar ratio of excess- $NH_4^+$  to  $NO_3^-$ .

exceeded 41  $\mu g$  m<sup>-3</sup> (the 95th percentile) for over two consecutive hours) are shown in Fig. 5a–(d). PM<sub>2.5</sub> levels were lowest at dawn, rising post-sunrise, peaking around 10 a.m., and then declining along with relative humidity (Fig. 5a). During the daytime, Ox (O<sub>3</sub>+NO<sub>2</sub>) and SO<sub>4</sub><sup>2</sup> concentrations concurrently rose, likely due to photochemical reactions driven by stronger solar radiation. However, these daytime increases in sulfates did not significantly impact overall PM<sub>2.5</sub> concentrations, indicating limited contribution from daytime photochemical SO<sub>4</sub><sup>2</sup> production to PM<sub>2.5</sub> levels. The minor midday PM<sub>2.5</sub> peak might also be influenced by the photochemical oxidation of VOCs producing particulate organic matter, but without measurements of organic matter, we cannot confirm its contribution in this study.

Both  $NO_3^-$  and  $NH_4^+$  concentrations mirrored the diurnal pattern of  $PM_{2.5}$ , which was opposite to that of temperature because high temperatures increase the equilibrium constant for the reactions of  $NH_3$  and  $HNO_3$  to form  $NH_4NO_3$  (R1), resulting in enhanced vaporization into the gas phase (Seinfeld and Pandis, 2016). Until the morning  $PM_{2.5}$  peak, low temperatures and high relative humidity promoted maximal ALWC, coinciding with sharp increases in inorganic ions such as nitrate, ammonium, and sulfate. These diurnal patterns suggest that the heterogeneous formation of SIA, alongside the onset of photochemical processes, likely drove increases in  $PM_{2.5}$  levels during periods of low to moderate concentrations. We also note that this  $PM_{2.5}$  peak period

aligned with peak traffic hours when the emissions of precursor gases were most active.

In ammonium-rich environments, the reaction between gaseous  $\rm HNO_3$  and  $\rm NH_3$  to form  $\rm NH_4NO_3$  is typically known as the primary pathway for  $\rm NO_3^-$  formation (Huang et al., 2011; Pathak et al., 2009). However, recent studies suggest that even in ammonium-rich environments, the dissolution of  $\rm N_2O_5$  into liquid aerosols followed by hydrolysis to form aqueous  $\rm HNO_3(aq)$  can be a significant pathway for elevated  $\rm NO_3^-$  levels (Lin et al., 2020; Peng et al., 2021), as presented in R(2) – R(4) (Brown and Stutz, 2012; Chang et al., 2011):

$$NO_{2(g)} + O_{3(g)} \rightarrow NO_3^- + O_{2(g)} (R 2)$$

$$NO_{2(g)} + NO_3^- \rightarrow N_2O_{5(g)} (R 3)$$

$$N_2O_{5(g)} + H_2O_{(l)} \rightarrow 2HNO_{3(aq)} (R 4)$$

The diurnal variations of relevant species during high  $PM_{2.5}$  periods in this study (>41  $\mu g m^{-3}$ , 95th percentile) also support the importance of heterogeneous SIA formation (particularly nitrates) in the elevation of  $PM_{2.5}$  levels. During these periods, nighttime rapid increases in SIA concentrations, such as nitrate and sulfate, were observed, followed by daytime declines. This pattern aligns closely with that of  $PM_{2.5}$  (Fig. 5e, g, and 5h). While daytime gas-phase  $HNO_3(g)$  formation involves  $NO_2$ 

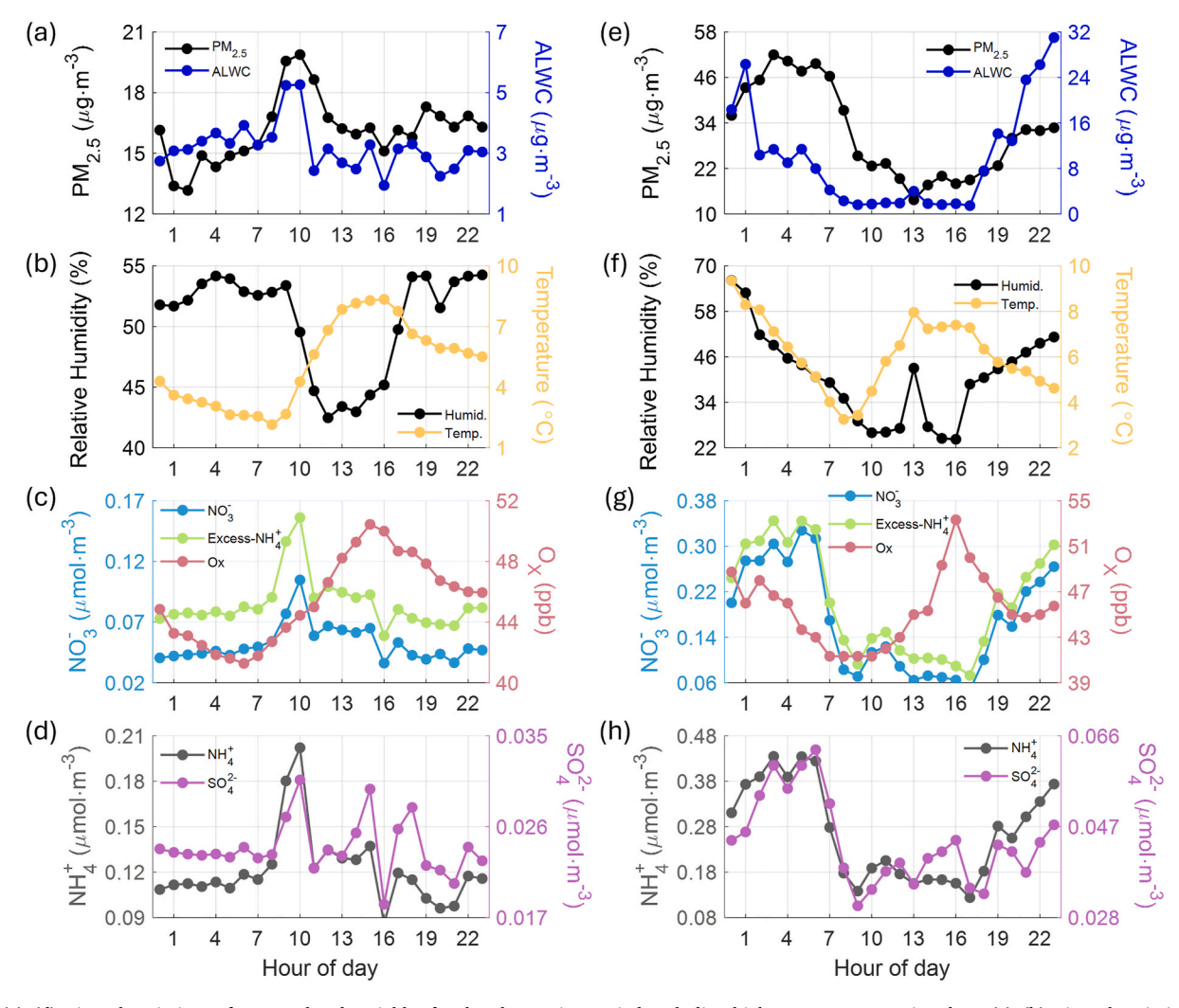


Fig. 5. (a)–(d) Diurnal variations of  $PM_{2.5}$ -related variables for the observation period excluding high  $PM_{2.5}$  concentration days. (e)–(h) Diurnal variations of the same species for days with high  $PM_{2.5}$  events (the upper 5 % concentrations (=41  $\mu$ g m<sup>-3</sup>) last for more than 2 h). (a) and (c) Black and blue lines represent  $PM_{2.5}$  mass concentrations and LWC, respectively. (b) and (f) Black and yellow lines represent RH and temperature, respectively. (c) and (g) Sky-blue, green and red lines represent  $NO_3^-$ , excess- $NH_4^+$ , and  $NC_3^+$  concentrations, respectively. (d) and (h) Gray and purple lines denote  $NC_3^+$  concentrations, respectively.

reacting with OH, this process is limited at night due to reduced OH concentrations. Particularly, our results showed that the sharp increase in nighttime relative humidity and ALWC preceded rises in SIA and  $PM_{2.5}$  concentrations, while daytime reductions in  $PM_{2.5}$  concentrations were accompanied by lower ALWC and relative humidity (Fig. 5e and f). Therefore, nighttime nitrate formation is expected to be driven primarily by heterogeneous processes during these periods. Lin et al. (2020) also corroborated that elevated ALWC during high  $PM_{2.5}$  pollution periods, associated with declining Ox concentrations, underscored the significance of  $N_2O_5$  hydrolysis for nocturnal nitrate formation. Consequently, in the coastal megacity of South Korea, enhanced ALWC facilitated by higher relative humidity due to low temperatures combined with an influx of water vapor, significantly contributed to the heterogeneous formation of SIA, particularly nitrate, profoundly influencing high  $PM_{2.5}$  concentrations during nighttime.

## 3.4. Evidence from ISORROPIA model results

To further substantiate the findings that elevated ALWC promoted heterogeneous nitrate formation during high  $PM_{2.5}$  events, we examined the relationship between gaseous  $HNO_3(g)$  (a precursor to nitrate) as calculated by the ISORROPIA model and the observed concentrations of particulate nitrate (Fig. 6). This model is well-documented for its proficiency in replicating the levels of inorganic ions and precursor gases as reported in previous studies (Brown and Stutz, 2012; Guo et al., 2016, 2017; Huang et al., 2011; Lin et al., 2020). The scatter plot in Fig. 6 delineates marked patterns between low and high nitrate concentrations. In conditions of elevated ALWC, the  $HNO_3(g)/NO_3^-$  ratios exhibited a reduced slope, suggesting a predominant partitioning of

nitrate into the particulate phase. In contrast, under lower ALWC conditions, the slope was steeper, indicating a propensity for nitrate to remain in the gas-phase (Fig. 6a). Moreover, under conditions of lower temperature and higher relative humidity, the slopes of  $\rm HNO_3(g)$  to  $\rm NO_3^-$  were reduced, further indicating the enhanced partitioning of nitrate into the condensed phase. These observations support the hypothesis that an increase in ALWC facilitated the formation of inorganic species, which led to an increase in  $\rm PM_{2.5}$  concentrations. Additionally, the  $\rm HNO_3/NO_3^-$  ratios with relatively high pH seem to be distributed along the lower slope line, indicating under high aerosol pH conditions, nitrates in the condensed phase dominate over the gas phase, as detailed by Guo et al. (2016).

## 3.5. A case study of high PM<sub>2.5</sub> concentration events

## 3.5.1. Evolution of surface area size distributions

In aerosol volume size distributions, the volume concentrations in accumulation mode can be directly converted into mass concentration, assuming uniform density, and thus can represent  $PM_{2.5}$  mass concentrations (Seinfeld and Pandis, 2016). However, during the measurement period, aerosol volume size distributions showed an unimodal pattern across most environments, with minimal variation in mode size, making it difficult to examine the formation processes based on mode size. Particle number size distributions, on the other hand, are directly influenced by local combustion sources, such as vehicle emissions, and are concentrated in smaller sizes, particularly below the Aitken mode. Thus, particle number size distributions have different characteristics in  $PM_{2.5}$  formation processes and variability when compared to  $PM_{2.5}$  mass concentrations (Choi et al., 2014; Seinfeld and Pandis, 2016).

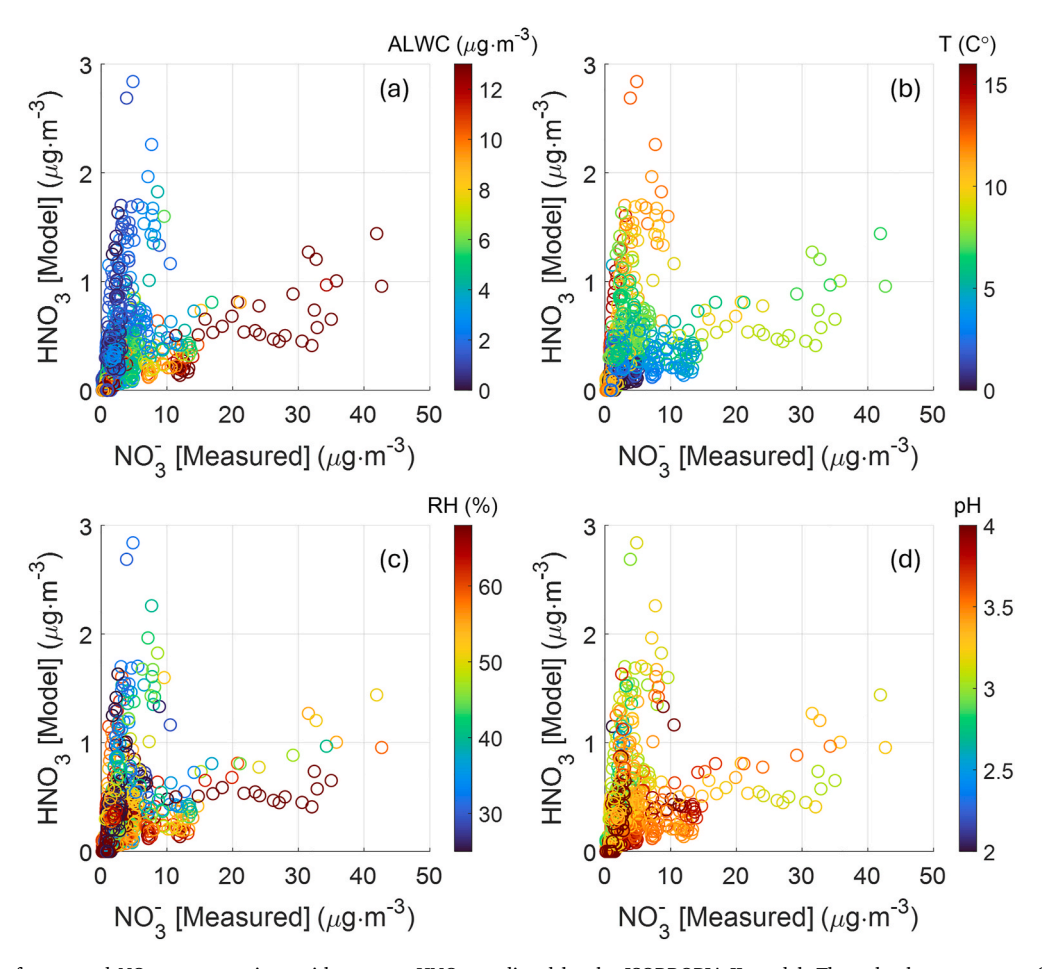


Fig. 6. Comparison of measured  $NO_3^-$  concentrations with gaseous HNO<sub>3</sub> predicted by the ISORROPIA-II model. The color bars represent (a) ALWC levels, (b) temperature, (c) relative humidity, and (d) pH.

In contrast, particle surface area concentrations are associated with  $PM_{2.5}$  growth, providing a surface for the condensation of precursor gases. In fact, observed particle surface area concentrations showed similar variability to that of  $PM_{2.5}$  mass concentrations (SI, Fig. S9). Moreover, unlike volume size distributions, surface area size distributions typically comprised 3–5 modes, making them useful for examining the evolution of each mode during the stage of increasing  $PM_{2.5}$ , and for linking with variations in chemical properties.

Four periods for this case study were selected where  $PM_{2.5}$  mass concentrations exceeded 35  $\mu g \cdot m^{-3}$  for at least two consecutive hours (SI, Fig. S9). The first case lasted from 2 p.m. on January 17 to 6 p.m. on January 18, and the second case spanned from January 19 to midnight on January 23. Rainfall occurred on January 22 but was a light drizzle with a precipitation rate of 0.4 mm/h, affecting minimally on  $PM_{2.5}$  concentrations (we did not see any abrupt drop in concentrations due to washout/rainout effects). The third case spanned from January 29 to 9 a.m. on January 31, and the fourth case from 3 p.m. on January 31 to 9 a.m. on February 2. Despite rainfall on Feb. 1 of the fourth case, both  $PM_{2.5}$  concentrations and surface area concentrations increased rapidly after the rain stopped.

During the selected cases, five aerosol modes were extracted from observed surface area size distributions with the fitting method described in Section 2.3. The modes were distinguished by their size: Mode 1 with diameter less than 50 nm, Mode 2 50–100 nm, Mode 3100–200 nm, Mode 4200–300 nm, and Mode 5 greater than 300 nm.

All cases shared some common features. First, the size of the most significant mode in surface area size distributions grew during the case periods (thick black line on the size distribution plots in Fig. 7). Second, in all cases, relative humidity (%), specific humidity (g/kg), and ALWC levels increased at the early stages of high  $PM_{2.5}$  events. Subsequently, nitrate concentrations (as representative inorganic ions due to their linear contribution to  $PM_{2.5}$  concentration increases) rose, followed by increases in  $PM_{2.5}$  concentrations (Fig. 7).

Here, we focus on Case 2 as the representative case due to space limitations, as it exhibited the longest continuous particle growth (Fig. 7b); other cases showed similar variation trends. Initially, the specific humidity, which had increased during the day, persisted into the night, and relative humidity increased due to the lower nighttime temperatures (as indicated by the gray box marked ① in the second plot of Fig. 7b). Subsequently, ALWC levels rose following the increase in

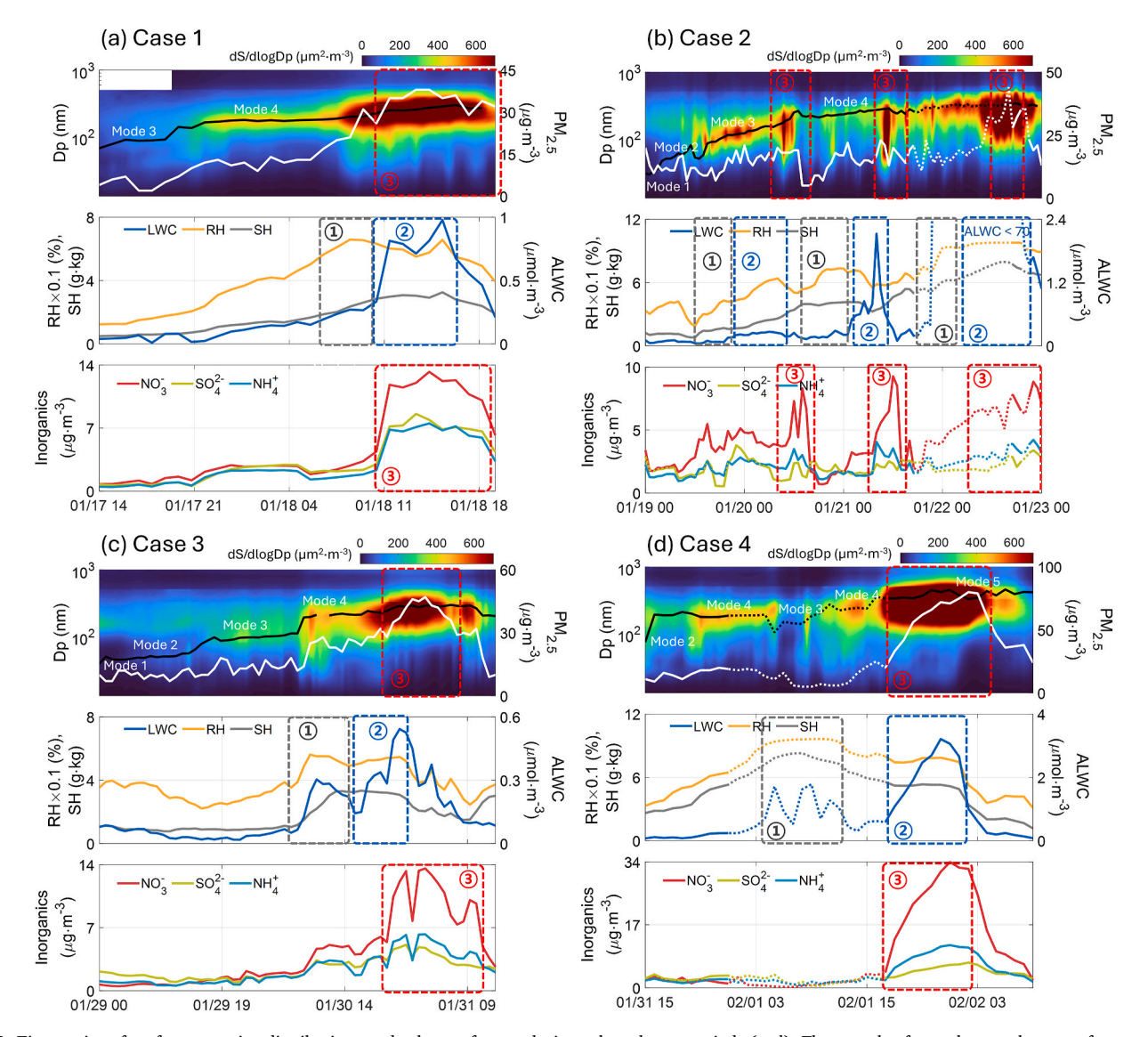


Fig. 7. Time series of surface area size distributions and relevant factors during selected case periods (a–d). The top plot for each case shows surface area size distributions, mode diameters of the major mode (black line), and PM<sub>2.5</sub> concentrations (white line). The middle plot displays relative humidity (yellow line), specific humidity (gray line), and ALWC (blue line). The bottom plot indicates concentrations of nitrate (red line), sulfate (light green line), and ammonium ions (sky blue line). The dotted lines in panel (d) mark the rainy periods.

relative humidity and specific humidity (blue box marked @ in the second plot of Fig. 7b). The modal sizes of the major modes in size distributions consistently increased through stages @ and @. Following stage @, where ALWC sharply increased, inorganic ions (especially nitrate) then increased (red box marked @ in the third plot of Fig. 7b). As aerosol surface area concentrations steadily grew, the size of the major aerosol mode also increased consistently. These evolutions of surface area size distributions, along with variations in meteorological conditions, ALWC, and inorganic ions, were consistently observed for the other cases. These common features imply that under the conditions of high relative humidity with sufficient water vapor concentrations, increased ALWC and growing aerosol surface areas facilitated the heterogeneous formation of SIA, consequently leading to an elevation in PM2.5 levels.

## 3.5.2. The sizes of dominant aerosol modes and PM<sub>2.5</sub> formation

Fig. 8 elucidates the relationships between the diameter of the largest major mode in the measured aerosol surface area size distributions and various associated factors, including  $PM_{2.5}$ , ALWC,  $NO_3^-$ , relative humidity (RH), NH $_3$ , and the condensational sink. The typical features observed in these comparisons include that when the smaller modes, modes 1 and 2 (below 100 nm), dominate, no clear correlation was observed between the mode size and  $PM_{2.5}$ , ALWC, or RH. However, as the major mode shifted to mode 3 or larger (100–200 nm or above), positive correlations became apparent with  $PM_{2.5}$ , ALWC, and RH.

Based on the results of cascade impactor measurements, John et al. (1990) identified the smallest mode in the mass size distributions (with a

diameter of  $0.2 \pm 0.1 \mu m$ ) as the condensation mode, formed by gas-phase reactions. They also referred to a mode with a diameter of 0.7  $\pm$  0.2  $\mu m$  as the droplet mode, which originates from the growth of the condensation mode due to the inclusion of water vapor (John et al., 1990). In this context, modes 1 and 2 in this study are considered to have weak correlations with ALWC and RH, because the dominant sources for these smallest modes are primary emissions or gas-phase reactions, rather than heterogeneous reactions facilitated by adding water vapor. Moreover, these smaller modes exert a minor impact on PM2.5 mass concentrations due to their tiny sizes, showing an insignificant relationship with PM<sub>2.5</sub>. In Cases 2 and 3, concentrations of NH<sub>3</sub> and NO<sub>3</sub> show a positive correlation with the size of modes 1 through 3. Additionally, the condensational sink (CS), which reflects particle growth by providing a surface for the condensation of precursor gases (Eq. S2-S4 in SI (Fuchs and Sutugin, 1971; Pirjola et al., 1999), also exhibits a positive correlation with the growth in mode size, suggesting that gas-phase reactions proposed by John et al. (1990) may have contributed to the growth of these smaller modes.

When the larger modes (modes 3–5) became dominant, the mode sizes and  $PM_{2.5}$  mass concentrations showed a strong positive correlation. In addition, the sizes of the dominant mode tended to grow as ALWC and RH increased, likely due to the transition from condensation mode to droplet mode through the addition of water vapor, as suggested by John et al. (1990). In the droplet mode, the importance of heterogeneous chemistry in  $PM_{2.5}$  formation may become more significant due to elevated ALWC. Furthermore, the increase in CS driven by the growth of larger dominant modes appeared to provide favorable conditions for

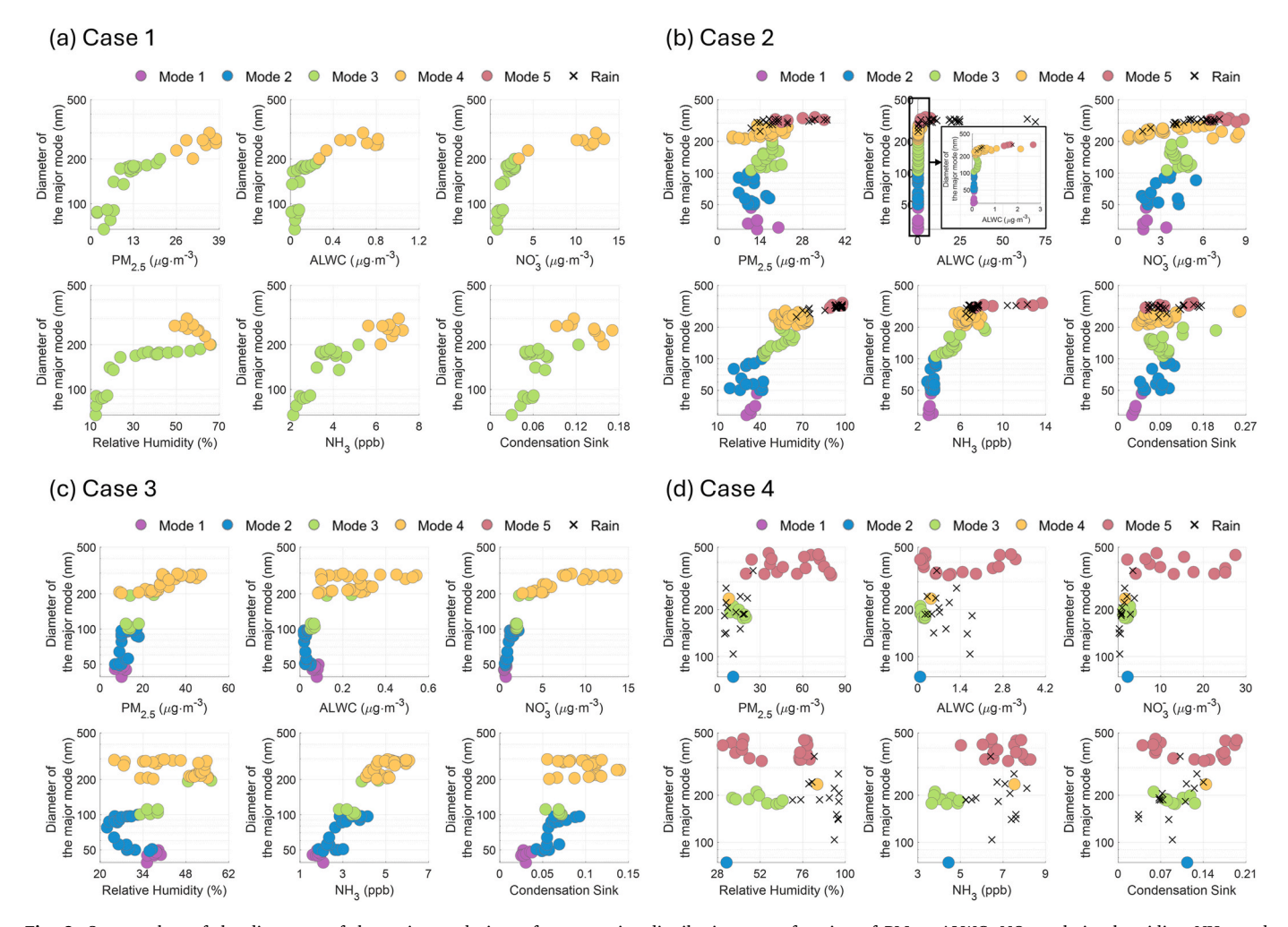


Fig. 8. Scatter plots of the diameters of the major mode in surface area size distributions as a function of  $PM_{2.5}$ , ALWC,  $NO_3^-$ , relative humidity,  $NH_3$ , and condensational sink. Colors represent the aerosol modes.

the condensation of water vapor and precursor gases. In particular, the increase in ALWC not only provides a greater volume of medium for the hydrolysis of precursor gases (Wang et al., 2020) but also dilutes hydrogen ions produced by acids, thereby raising the aerosol's pH (Arsene et al., 2011). Under high pH conditions, nitrates prefer to exist in the condensed phase (Guo et al., 2016). All these conditions can facilitate the heterogeneous formation of nitrates.

The concentrations of ammonia, a major precursor gas, also increased as the mode size grew, indicating that ammonia also plays a significant role in the growth of  $PM_{2.5}$ . However, Case 4 showed a less pronounced relationship compared to Cases 1–3. In Case 4, the rainfall event occurred (indicated by dotted lines in Fig. 8d) just before the abrupt and sharp increase in  $PM_{2.5}$  concentrations, suggesting a potential influence from the rain. Alternatively, the sudden advent of high  $PM_{2.5}$  concentrations following the rainfall event may also be attributed to the influence of long-range transport following a weather front (Kang et al., 2019). During this period, a weak yellow dust (or Asian dust) event was recorded, representing distinct environmental characteristics (AirKorea, 2021).

#### 4. Conclusion

To investigate the physical and chemical characteristics of  $PM_{2.5}$  and their formation mechanism during wintertime high-concentration events in a coastal megacity in Korea, field measurements were conducted from January 13 to February 7, 2021, in Busan, the second-largest city on the south coast of Korea. One of the major findings is that as  $PM_{2.5}$  concentrations increased; the proportion of sulfate decreased while that of nitrate increased. This shift underscores the growing importance of nitrate in SIAs as  $SO_2$  concentrations decline, potentially due to effective SO2 mitigation policies in the port cities. Historically, the dominant SIA component in coastal port cities in Korea, including Busan, was sulfate during high  $PM_{2.5}$  events (Kim et al., 2020). This highlights the need for the transition to the next stage of pollution policy aimed at curbing nitrate production in Korea's coastal port cities.

The measurement site exhibited ammonium-rich environments where most sulfates (SO $_4^2$ ) and nitrates (NO $_3$ ) were fully neutralized by ammonium (NH $_4^+$ ). The diurnal variations of PM $_{2.5}$  and associated variables during high PM $_{2.5}$  periods showed that nighttime peaks in relative humidity (RH), which was driven by both the increase in specific humidity and lowered temperature, and ALWC precede increases in inorganic ion concentrations, leading to the nighttime PM $_{2.5}$  peak. The ISORROPIA-II model results support this by presenting that lower HNO $_3$ (g)/NO $_3$  ratios are associated with relatively higher ALWC, lower temperatures, and higher RH, indicating that nitrates predominantly exist in the particle phase under these conditions. These findings suggest that in Korea's port cities with ammonium-rich environments, the wintertime increase in PM $_{2.5}$  concentrations is primarily driven by the formation of inorganic ions, particularly nitrates, through heterogeneous chemistry rather than daytime photochemistry.

A distinctive approach of this study is that it explores the common features in the developing stages of high-concentration PM2.5 events through case studies, linking particle surface area size distributions with factors associated with PM2.5 formation. Four case studies highlighted that increases in relative and specific humidity preceded the augmentation of ALWC with growth of the major mode in aerosol surface area size distributions, which was extracted via fitting a multi-log-normal distribution function to observed aerosol size distributions. The growth of the major mode in surface area size distributions correlated with increases in ammonia, condensational sink, and nitrate concentrations, alongside RH and ALWC. The increases in ALWC and aerosol surface area can provide a greater medium volume for the hydrolysis of precursor gases and simultaneously raise the aerosol's pH. All these conditions favor the presence of nitrates in the condensed phase through heterogeneous processes, thereby facilitating enhanced nitrate formation during nighttime.

Consequently, our findings suggest that high  $PM_{2.5}$  levels in the coastal megacity in South Korea were driven by the heterogeneous chemistry of inorganic ions, particularly through nitrate formation. As  $SO_2$  emissions are expected to continue decreasing due to strict reduction policies in Korean port cities, the role of nitrate is likely to become increasingly pivotal, especially in ammonium-rich environments. Therefore, to effectively mitigate  $PM_{2.5}$  levels in Korea's coastal urban areas, integrated strategies that reduce both  $NO_X$  and  $NH_3$  emissions are required. Unfortunately,  $NH_3$  emission sources in this port megacity were not identified in this study. Thus, the sources and emission inventory of  $NH_3$  need to be more accurately quantified alongside continuous monitoring of its concentrations.

## CRediT authorship contribution statement

Yongmi Park: Visualization, Investigation, Writing – original draft, Validation, Formal analysis. Myounghwa Byun: Validation, Formal analysis, Investigation. Jaehun Park: Investigation. Subin Han: Visualization, Formal analysis, Investigation. Jae-Jin Kim: Funding acquisition, Writing – review & editing. Youn-Suk Son: Resources, Investigation, Methodology. Taehyoung Lee: Writing – review & editing, Methodology. Wonsik Choi: Validation, Conceptualization, Supervision, Investigation, Project administration, Writing – review & editing.

## **Declaration of competing interest**

The authors declare that they have no known competing financial interests or personal relationships that could have appeared to influence the work reported in this paper.

## Acknowledgement

This work was supported by the FRIEND (Fine Particle Research Initiative in East Asia Considering National Differences) Project through the National Research Foundation of Korea (NRF) funded by the Ministry of Science and ICT [grant number 2020M3G1A1115001], R&D Program for Forest Science Technology provided by Korea Forest Service (Korea Forestry Promotion Institute) [grant number 2022428C10-2324-0802], and the Basic Science Research Program through the NRF funded by the Ministry of Education [RS-2024-00341302]. This work was also partially supported by a grant from the National Institute of Environment Research, funded by the Ministry of Environment of the Republic of Korea [grant number NIER-2021-03-03-007]. Inorganic ions were measured using the particle into liquid sampler-ion chromatography (PILS-IC) system managed by the Integrated Analytical Center for Earth and Environmental Sciences of Pukyong National University.

## Appendix A. Supplementary data

Supplementary data to this article can be found online at https://doi.org/10.1016/j.atmosenv.2025.121435.

## Data availability

Data will be made available on request.

## References

AirKorea, 2021. Air quality forecasts and alerts. https://www.airkorea.or.kr/web/dustForecast?pMENU\_NO=113. (Accessed 27 September 2024).

Arsene, C., Olariu, R.I., Zarmpas, P., Kanakidou, M., Mihalopoulos, N., 2011. Ion composition of coarse and fine particles in Iasi, north-eastern Romania: implications for aerosols chemistry in the area. Atmos. Environ. 45, 906–916. https://doi.org/10.1016/i.atmosenv.2010.11.013.

Bae, C., Kim, B.U., Kim, H.C., Yoo, C., Kim, S., 2020. Long-range transport influence on key chemical components of PM<sub>2.5</sub> in the Seoul metropolitan area, South Korea,

- during the years 2012-2016. Atmosphere 11. https://doi.org/10.3390/
- Bae, M., Kim, B.U., Kim, H.C., Woo, J.H., Kim, S., 2022. An observation-based adjustment method of regional contribution estimation from upwind emissions to downwind PM<sub>2.5</sub> concentrations. Environ. Int. 163. https://doi.org/10.1016/j. envirt 2022 107214
- Bian, Y.X., Zhao, C.S., Ma, N., Chen, J., Xu, W.Y., 2014. A study of aerosol liquid water content based on hygroscopicity measurements at high relative humidity in the North China Plain. Atmos. Chem. Phys. 14, 6417–6426. https://doi.org/10.5194/ acp-14-6417-2014.
- Bougiatioti, A., Nikolaou, P., Stavroulas, I., Kouvarakis, G., Weber, R., Nenes, A., Kanakidou, M., Mihalopoulos, N., 2016. Particle water and pH in the eastern Mediterranean: source variability and implications for nutrient availability. Atmos. Chem. Phys. 16, 4579–4591. https://doi.org/10.5194/acp-16-4579-2016.
- Brown, S.S., Stutz, J., 2012. Nighttime radical observations and chemistry. Chem. Soc. Rev. 41, 6405–6447. https://doi.org/10.1039/c2cs35181a.
- Capss. https://www.air.go.kr/capss/emission/search.do?menuId=33, 2022-. (Accessed 28 March 2025).
- Chang, W.L., Bhave, P.V., Brown, S.S., Riemer, N., Stutz, J., Dabdub, D., 2011. Heterogeneous atmospheric chemistry, ambient measurements, and model calculations of N<sub>2</sub>O<sub>5</sub>: a review. Aerosol Sci. Technol. 45, 665–695. https://doi.org/ 10.1080/02786826.2010.551672.
- Chen, Z., Guan, H., Tian, J., 2024. Long-term change in winter aerosol composition and sources in Guiyang Southwest China (2003–2020). Atmos. Pollut. Res. 15. https:// doi.org/10.1016/j.apr.2024.102263.
- Choi, W., Paulson, S.E., 2016. Closing the ultrafine particle number concentration budget at road-to-ambient scale: implications for particle dynamics. Aerosol Sci. Technol. 50, 448–461. https://doi.org/10.1080/02786826.2016.1155104.
- Choi, W., Winer, A.M., Paulson, S.E., 2014. Factors controlling pollutant plume length downwind of major roadways in nocturnal surface inversions. Atmos. Chem. Phys. 14, 6925–6940. https://doi.org/10.5194/acp-14-6925-2014.
- Erisman, J.W., Schaap, M., 2004. The need for ammonia abatement with respect to secondary PM reductions in Europe. Environ. Pollut. 129, 159–163. https://doi.org/ 10.1016/j.envpol.2003.08.042.
- Fang, Z., Dong, S., Huang, C., Jia, S., Wang, F., Liu, H., Meng, H., Luo, L., Chen, Y., Zhang, H., Li, R., Zhu, Y., Tang, M., 2025. On using an aerosol thermodynamic model to calculate aerosol acidity of coarse particles. J. Environ. Sci. 148, 46–56. https:// doi.org/10.1016/j.ies.2023.07.001.
- Fountoukis, C., Nenes, A., 2007. Isorropia II: a computationally efficient thermodynamic equilibrium model for  $K^+$ -Ca<sup>2+</sup>-Mg<sup>2+</sup>-NH $_4^+$ -Na<sup>+</sup>-SO $_4^2$ -NO $_3$ -Cl<sup>-</sup>-H $_2$ O aerosols. Atmos. Chem. Phys. 7, 4639–4659. https://doi.org/10.5194/acp-7-4639-2007.
- Fuchs, N.A., Sutugin, A.G., 1971. High-dispersed aerosols. Int. Rev. Aerosol Phys. Chem. 2, 1–60. https://doi.org/10.1016/B978-0-08-016674-2.50006-6.
- Ge, X., Li, L., Chen, Y., Chen, H., Wu, D., Wang, J., Xie, X., Ge, S., Ye, Z., Xu, J., Chen, M., 2017. Aerosol characteristics and sources in Yangzhou, China resolved by offline aerosol mass spectrometry and other techniques. Environ. Pollut. 225, 74–85. https://doi.org/10.1016/j.envpol.2017.03.044.
- Goodman, A.L., Underwood, G.M., Grassian, V.H., 2000. A laboratory study of the heterogeneous reaction of nitric acid on calcium carbonate particles. J. Geophys. Res. 105, 29053–29064. https://doi.org/10.1029/2000JD900396.
- Griffith, S.M., Huang, X.H.H., Louie, P.K.K., Yu, J.Z., 2015. Characterizing the thermodynamic and chemical composition factors controlling PM2.5 nitrate: insights gained from two years of online measurements in Hong Kong. Atmos. Environ. 122, 864–875. https://doi.org/10.1016/j.atmosenv.2015.02.009.
- Guo, H., Xu, L., Bougiatioti, A., Cerully, K.M., Capps, S.L., Hite, J.R., Carlton, A.G., Lee, S. H., Bergin, M.H., Ng, N.L., Nenes, A., Weber, R.J., 2015. Fine-particle water and pH in the southeastern United States. Atmos. Chem. Phys. 15, 5211–5228. https://doi.org/10.5194/acp.15-5211-2015
- Guo, H., Sullivan, A.P., Campuzano-Jost, P., Schroder, J.C., Lopez-Hilfiker, F.D., Dibb, J. E., Jimenez, J.L., Thornton, J.A., Brown, S.S., Nenes, A., Weber, R.J., 2016. Fine particle pH and the partitioning of nitric acid during winter in the northeastern United States. J. Geophys. Res. Atmos. 121, 10355–10376. https://doi.org/10.1002/2016JD025311.
- Guo, H., Weber, R.J., Nenes, A., 2017. High levels of ammonia do not raise fine particle pH sufficiently to yield nitrogen oxide-dominated sulfate production. Sci. Rep. 7. https://doi.org/10.1038/s41598-017-11704-0.
- Guo, H., Otjes, R., Schlag, P., Kiendler-Scharr, A., Nenes, A., Weber, R.J., 2018. Effectiveness of ammonia reduction on control of fine particle nitrate. Atmos. Chem. Phys. 18, 12241–12256. https://doi.org/10.5194/acp-18-12241-2018.
- Gysel, M., Crosier, J., Topping, D.O., Whitehead, J.D., Bower, K.N., Cubison, M.J., Williams, P.I., Flynn, M.J., McFiggans, G.B., Coe, H., 2007. Closure study between chemical composition and hygroscopic growth of aerosol particles during TORCH2. Atmos. Chem. Phys. 7, 6131–6144. https://doi.org/10.5194/acp-7-6131-2007.
- Han, S.H., Kim, Y.P., 2015. Long-term trends of the concentrations of mass and chemical composition in PM<sub>2.5</sub> over Seoul. J. Korean Soc. Atmos. Environ. 31, 143–156. https://doi.org/10.5572/kosae.2015.31.2.143.
- Hennigan, C.J., Izumi, J., Sullivan, A.P., Weber, R.J., Nenes, A., 2015. A critical evaluation of proxy methods used to estimate the acidity of atmospheric particles. Atmos. Chem. Phys. 15, 2775–2790. https://doi.org/10.5194/acp-15-2775-2015.
- Huang, X., Qiu, R., Chan, C.K., Kant, P.R., 2011. Evidence of high  $PM_{2.5}$  strong acidity in ammonia-rich atmosphere of Guangzhou, China: transition in pathways of ambient ammonia to form aerosol ammonium at  $[NH^{\downarrow}_{+}]/[SO_4^2]=1.5$ . Atmos. Res. 99, 488–495. https://doi.org/10.1016/j.atmosres.2010.11.021.
- Hussein, T., Maso, M., Petäjä, T., Koponen, I.K., Paatero, P., Aalto, P.P., Hämeri, K., Kulmala, M., 2005. Evaluation of an automatic algorithm for fitting the particle number size distributions, Boreal env. Res. 10, 337–355.

- Hwang, K., Kim, J., Lee, J.Y., Park, J.S., Park, S., Lee, G., Kim, C.H., Kim, P., Shin, S.H., Lee, K.Y., An, J.Y., Park, J., Kim, J.B., 2023. Physicochemical characteristics and seasonal variations of PM<sub>2.5</sub> in urban, industrial, and suburban areas in South Korea. Asian J. Atmos. Environ. 17. https://doi.org/10.1007/s44273-023-00018-5.
- Jo, Y.J., Lee, H.J., Jo, H.Y., Woo, J.H., Kim, Y., Lee, T., Heo, G., Park, S.M., Jung, D., Park, J., Kim, C.H., 2020. Changes in inorganic aerosol compositions over the yellow sea area from impact of Chinese emissions mitigation. Atmos. Res. 240. https://doi. org/10.1016/j.atmosres.2020.104948.
- John, W., Wall, S.M., Ondo, J.L., Winklmayr, W., 1990. Modes in the size distributions of atmospheric inorganic aerosol. Atmos. Environ. A. Gen. Top. 24, 2349–2359. https://doi.org/10.1016/0960-1686(90)90327-J.
- Kang, H., Zhu, B., Gao, J., He, Y., Wang, H., Su, J., Pan, C., Zhu, T., Yu, B., 2019. Potential impacts of cold frontal passage on air quality over the Yangtze River Delta, China. Atmos. Chem. Phys. 19, 3673–3685. https://doi.org/10.5194/acp-19-3673-2019
- Kang, S., Park, G., Park, T., Ban, J., Kim, K., Seo, Y., Choi, J., Seo, S., Choi, J., Bae, M.S., Lee, T., 2020. Semi-continuous measurements of water-soluble organic carbon and ionic composition of PM<sub>2.5</sub> in Baengnyeong Island during the 2016 KORUS-AQ (Korea-United States air quality Study). Asian J. Atmos. Environ. 14, 307–318. https://doi.org/10.5572/ajae.2020.14.3.307.
- Kang, S., Choi, S., Ban, J., Kim, K., Singh, R., Park, G., Kim, M.B., Yu, D.G., Kim, J.A., Kim, S.W., Park, M.S., Kim, C.H., Lee, M., Heo, G., Jang, Y.W., Ha, S.S., Park, T., Lee, T., 2022. Chemical characteristics and sources of PM<sub>2.5</sub> in the urban environment of Seoul, Korea. Atmos. Pollut. Res. 13. https://doi.org/10.1016/j.anr.2022.101568.
- Khlystov, A., Stanier, C., Pandis, S.N., 2004. An algorithm for combining electrical mobility and aerodynamic size distributions data when measuring ambient aerosol. Aerosol Sci. Technol. 38, 229–238. https://doi.org/10.1080/02786820390229543.
- Kim, J.-M., Jo, Y.-J., Yang, G.-H., Heo, G., Kim, C.-H., 2020. Analysis of recent trends of particulate matter observed in Busan - comparative study on Busan vs. Seoul metropolitan area (I). J. Environ. Sci. Int. 29, 177–189. https://doi.org/10.5322/ jesi.2020.29.2.177.
- Kim, D., Foy, B., Kim, H., 2022. The investigations on organic sources and inorganic formation processes and their implications on haze during late winter in Seoul, Korea. Environ. Res. 212. https://doi.org/10.1016/j.envres.2022.113174.
- Lee, T., Yu, X.Y., Kreidenweis, S.M., Malm, W.C., Collett, J.L., 2008. Semi-continuous measurement of PM<sub>2.5</sub> ionic composition at several rural locations in the United States. Atmos. Environ. 42, 6655–6669. https://doi.org/10.1016/j. atmosenv.2008.04.023.
- Lee, H., Gil, J., Lee, M., 2023. Characteristics of PM<sub>2.5</sub> composition and precursor gases in urban Seoul during 2021~2022. J. Korean Soc. Atmos. Environ. 39, 525–534. https://doi.org/10.5572/KOSAE.2023.39.4.525.
- Lin, Y.C., Zhang, Y.L., Fan, M.Y., Bao, M., 2020. Heterogeneous formation of particulate nitrate under ammonium-rich regimes during the high-PM<sub>2.5</sub> events in Nanjing, China, Atmos. Chem. Phys. 20, 3999–4011. https://doi.org/10.5194/acp-20-3999-2020
- Liu, M., Song, Y., Zhou, T., Xu, Z., Yan, C., Zheng, M., Wu, Z., Hu, M., Wu, Y., Zhu, T., 2017. Fine particle pH during severe haze episodes in northern China. Geophys. Res. Lett. 44, 5213–5221. https://doi.org/10.1002/2017GL073210.
- Ministry of Environment (ME), 2019. Comprehensive plan for particle matter management [2020 ~ 2024]. https://www.me.go.kr/home/web/policy\_data/read.do?menuId=10262&seq=7399. (Accessed 19 September 2024).
- Ministry of Oceans and Fisheries (MOF), 2019. Enforcement decree of the special act on the improvement of air quality in port areas. https://www.mof.go.kr/doc/ko/s electDoc.do?menuSeq=971&bbsSeq=10&docSeq=27072. (Accessed 19 September 2024).
- National institute of environmental research (NIER), 2019. Annual report on air quality. https://www.airkorea.or.kr/web/detailViewDown?pMENU\_NO=125. (Accessed 19 September 2024), 2020 (in Korean.
- National institute of environmental research (NIER), 2021. Annual report on air quality. https://www.airkorea.or.kr/web/detailViewDown?pMENU\_NO=125. (Accessed 19 September 2024), 2022.
- Nenes, A., Pandis, S.N., Weber, R.J., Russell, A., 2020. Aerosol pH and liquid water content determine when particulate matter is sensitive to ammonia and nitrate availability. Atmos. Chem. Phys. 20, 3249–3258. https://doi.org/10.5194/acp-20-3249-2020.
- Park, D.J., Ahn, J.Y., Shin, H.J., Bae, M.S., 2014. Characteristics of PM<sub>2.5</sub> carbonaceous aerosol using PILS-TOC and GC/MS-TD in Seoul. J. Korean Soc. Atmos. Environ. 30, 461–476. https://doi.org/10.5572/kosae.2014.30.5.461.
- Pathak, R.K., Louie, P.K.K., Chan, C.K., 2004a. Characteristics of aerosol acidity in Hong Kong. Atmos. Environ. 38, 2965–2974. https://doi.org/10.1016/j.atmosenv.2004.02.044.
- Pathak, R.K., Yao, X., Chan, C.K., 2004b. Sampling artifacts of acidity and ionic species in  $PM_{2.5}$ . Environ. Sci. Technol. 38, 254–259. https://doi.org/10.1021/es0342244. Pathak, R.K., Wu, W.S., Wang, T., 2009. Summertime  $PM_{2.5}$  ionic species in four major
- cities of China: nitrate formation in an ammonia-deficient atmosphere. Atmos. Chem. Phys. 9, 1711–1722. https://doi.org/10.5194/acp-9-1711-2009.
- Peng, J., Hu, M., Shang, D., Wu, Z., Du, Z., Tan, T., Wang, Y., Zhang, F., Zhang, R., 2021. Explosive secondary aerosol formation during severe haze in the North China Plain. Environ. Sci. Technol. 55, 2189–2207. https://doi.org/10.1021/acs.est.0c07204.
- Pirjola, L., Kulmala, M., Wilck, M., Bischoff, A., Stratmann, F., Otto, E., 1999. Formation of sulphuric acid aerosols and cloud condensation nuclei: an expression for significant nucleation and model comparison. J. Aerosol Sci. 30, 1079–1094. https://doi.org/10.1016/S0021-8502(98)00776-9.
- Seinfeld, J.H., Pandis, S.N., 2016. Atmospheric Chemistry and Physics, third ed. John Wiley & Sons, Inc., New Jersey.

- Seo, J., Lim, Y.B., Youn, D., Kim, J.Y., Jin, H.C., 2020. Synergistic enhancement of urban haze by nitrate uptake into transported hygroscopic particles in the Asian continental outflow. Atmos. Chem. Phys. 20, 7575–7594. https://doi.org/10.5194/ acp-20-7575-2020
- Squizzato, S., Masiol, M., Brunelli, A., Pistollato, S., Tarabotti, E., Rampazzo, G., Pavoni, B., 2013. Factors determining the formation of secondary inorganic aerosol: a case study in the Po Valley (Italy). Atmos. Chem. Phys. 13, 1927–1939. https://doi. org/10.5194/acp-13-1927-2013.
- Uno, I., Wang, Z., Itahashi, S., Yumimoto, K., Yamamura, Y., Yoshino, A., Takami, A., Hayasaki, M., Kim, B.G., 2020. Paradigm shift in aerosol chemical composition over regions downwind of China. Sci. Rep. 10. https://doi.org/10.1038/s41598-020-63592-6.
- Vu, T.V., Shi, Z., Cheng, J., Zhang, Q., He, K., Wang, S., Harrison, R.M., 2019. Assessing the impact of clean air action on air quality trends in Beijing using a machine learning technique. Atmos. Chem. Phys. 19, 11303–11314. https://doi.org/ 10.5194/acp-19-11303-2019.
- Wang, W., Yu, J., Cui, Y., He, J., Xue, P., Cao, W., Ying, H., Gao, W., Yan, Y., Hu, B., Xin, J., Wang, L., Liu, Z., Sun, Y., Ji, D., Wang, Y., 2018. Characteristics of fine particulate matter and its sources in an industrialized coastal city, Ningbo, Yangtze River Delta, China. Atmos. Res. 203, 105–117. https://doi.org/10.1016/j.atmosres.2017.11.033.
- Wang, Y., Chen, Y., Wu, Z., Shang, D., Bian, Y., Du, Z., Schmitt, S.H., Su, R., Gkatzelis, G. I., Schlag, P., Hohaus, T., Voliotis, A., Lu, K., Zeng, L., Zhao, C., Alfarra, M.R., McFiggans, G., Wiedensohler, A., Kiendler-Scharr, A., Zhang, Y., Hu, M., 2020. Mutual promotion between aerosol particle liquid water and particulate nitrate enhancement leads to severe nitrate-dominated particulate matter pollution and low visibility. Atmos. Chem. Phys. 20, 2161–2175. https://doi.org/10.5194/acp-20-2161-2020
- Wang, J., Gao, J., Che, F., Wang, Y., Lin, P., Zhang, Y., 2022. Decade-long trends in chemical component properties of PM<sub>2.5</sub> in Beijing, China (2011–2020). Sci. Total Environ. 832. https://doi.org/10.1016/j.scitotenv.2022.154664.

- Xu, Q., Wang, S., Jiang, J., Bhattarai, N., Li, X., Chang, X., Qiu, X., Zheng, M., Hua, Y., Hao, J., 2019. Nitrate dominates the chemical composition of PM<sub>2.5</sub> during haze event in Beijing, China. Sci. Total Environ. 689, 1293–1303. https://doi.org/ 10.1016/j.scitotenv.2019.06.294.
- Ye, Z., Liu, J., Gu, A., Feng, F., Liu, Y., Bi, C., Xu, J., Li, L., Chen, H., Chen, Y., Dai, L., Zhou, Q., Ge, X., 2017. Chemical characterization of fine particulate matter in Changzhou, China, and source apportionment with offline aerosol mass spectrometry. Atmos. Chem. Phys. 17, 2573–2592. https://doi.org/10.5194/acp-17-2573-2017
- Zang, H., Zhao, Y., Huo, J., Zhao, Q., Fu, Q., Duan, Y., Shao, J., Huang, C., An, J., Xue, L., Li, Z., Li, C., Xiao, H., 2022. High atmospheric oxidation capacity drives wintertime nitrate pollution in the eastern Yangtze River Delta of China. Atmos. Chem. Phys. 22, 4355–4374. https://doi.org/10.5194/acp-22-4355-2022.
- Zhang, Q., Jimenez, J.L., Worsnop, D.R., Canagaratna, M., 2007. A case study of urban particle acidity and its influence on secondary organic aerosol. Environ. Sci. Technol. 41, 3213–3219. https://doi.org/10.1021/es061812j.
- Zhang, H., Li, R., Huang, C., Li, X., Dong, S., Wang, F., Li, T., Chen, Y., Zhang, G., Ren, Y., Chen, Q., Huang, R.-j., Chen, S., Xue, T., Wang, X., 2023. Seasonal variation of aerosol iron solubility in coarse and fine particles at an inland city in northwestern China. Atmos. Chem. Phys. 23, 3543–3559. https://doi.org/10.5194/acp-23-3543-2023
- Zheng, B., Tong, D., Li, M., Liu, F., Hong, C., Geng, G., Li, H., Li, X., Peng, L., Qi, J., Yan, L., Zhang, Y., Zhao, H., Zheng, Y., He, K., Zhang, Q., 2018. Trends in China's anthropogenic emissions since 2010 as the consequence of clean air actions. Atmos. Chem. Phys. 18, 14095–14111. https://doi.org/10.5194/acp-18-14095-2018.
- Zhou, M., Nie, W., Qiao, L., Huang, D.D., Zhu, S., Lou, S., Wang, H., Wang, Q., Tao, S., Sun, P., Liu, Y., Xu, Z., An, J., Yan, R., Su, H., Huang, C., Ding, A., Chen, C., 2022. Elevated formation of particulate nitrate from N<sub>2</sub>O<sub>5</sub> hydrolysis in the Yangtze River Delta region from 2011 to 2019. Geophys. Res. Lett. 49. https://doi.org/10.1029/2021GI.097393.